

High non-inductive fraction H-mode discharges generated by high-harmonic fast wave heating and current drive in the National Spherical Torus Experiment

G. Taylor,¹ J. C. Hosea,¹ C. E. Kessel,¹ B. P. LeBlanc,¹ D. Mueller,¹ C. K. Phillips,¹ E. J. Valeo,¹ J. R. Wilson,¹ P. M. Ryan,² P. T. Bonoli,³ J. C. Wright,³ and R. W. Harvey⁴

¹Princeton Plasma Physics Laboratory, Princeton, New Jersey 08543, USA

²Oak Ridge National Laboratory, Oak Ridge, Tennessee 37831, USA

³Plasma Science and Fusion Center, MIT, Massachusetts 02139, USA

⁴CompX, Del Mar, California 92014, USA

(Received 31 January 2012; accepted 15 March 2012; published online 4 April 2012)

A deuterium H-mode discharge with a plasma current of 300 kA, an axial toroidal magnetic field of 0.55 T, and a calculated non-inductive plasma current fraction of 0.7–1 has been generated in the National Spherical Torus Experiment by 1.4 MW of 30 MHz high-harmonic fast wave (HHFW) heating and current drive. Seventy-five percent of the non-inductive current was generated inside an internal transport barrier that formed at a normalized minor radius ~ 0.4 . Three quarters of the non-inductive current was bootstrap current, and the remaining non-inductive current was generated directly by HHFW power inside a normalized minor radius ~ 0.2 . © 2012 American Institute of Physics. [<http://dx.doi.org/10.1063/1.3699364>]

I. INTRODUCTION

The first experiments to generate high-confinement, or H-mode,¹ plasmas in a tokamak using ion cyclotron range of frequency (ICRF) fast-wave heating alone were conducted in ASDEX in 1986 where ICRF power heated a deuterium plasma with a hydrogen minority.² Several years later, H-mode plasmas were generated in DIII-D (Ref. 3) by direct fast-wave heating of electrons, via Landau damping and transit time magnetic pumping.^{4,5} Fast-wave generated H-mode plasmas are now studied extensively in conventional larger aspect ratio tokamaks, such as Alcator C-mod,⁶ and ICRF fast-wave heating will heat the deuterium and tritium in ITER H-mode discharges^{7,8} to nuclear fusion temperatures. In this paper, we present results for deuterium H-mode discharges generated and sustained by high-harmonic fast-wave (HHFW) heating in the National Spherical Torus Experiment (NSTX),⁹ a low aspect ratio, spherical torus (ST) device. The ICRF heating in these experiments used current drive antenna phasing and was predominantly via direct fast-wave heating of electrons.

ST devices offer several advantages compared to conventional, larger aspect ratio, tokamaks, including a high ratio of plasma to confining magnetic field pressure, compact geometry, good confinement, and relatively low confining magnetic field.¹⁰ But because of the constraints imposed by the STs compact geometry, it is critical to develop discharge initiation, plasma current (I_p) ramp-up, and plasma sustainment techniques that do not require a central solenoid. TSC (Ref. 11) simulations of non-solenoidal plasma scenarios in NSTX (Ref. 12) predict that HHFW heating¹³ can play an important role in enabling the generation of an H-mode ST discharge with a high fraction of non-inductive plasma current, $f_{NI} \geq 1$.

The $f_{NI} \geq 1$ strategy developed for NSTX includes coupling 5–6 MW of HHFW power (P_{RF}) into a non-inductive,

$I_p = 250 - 350$ kA, discharge that has been generated by coaxial helicity injection,¹⁴ outer poloidal field start-up,¹⁵ or plasma guns.¹⁶ The HHFW heating will be used to drive I_p from ~ 300 kA to ~ 500 kA through the generation of an H-mode plasma with substantial bootstrap current (I_{BS}) and direct fast-wave current drive (I_{FWCD}). At $I_p \sim 500$ kA, 90 keV deuterium fast ions from neutral beam injection (NBI) are sufficiently well confined in NSTX to heat the plasma and generate additional bootstrap current and neutral beam injection current drive.

The initial approach to developing this $f_{NI} \geq 1$ I_p ramp-up strategy on NSTX has been to heat a $I_p = 250 - 300$ kA flat top, inductively generated, deuterium plasma with HHFW power in order to drive the plasma into an H-mode with $f_{NI} \geq 1$. The first attempt at such an experiment was conducted on NSTX in 2005;¹⁷ the experiment used $P_{RF} \sim 2.7$ MW to heat a $I_p = 250$ kA, $B_T(0) = 0.45$ T plasma. These first experiments used an undirected antenna launch spectrum so that there was no directly generated FWCD, only bootstrap current. H-mode discharges with a calculated $f_{NI} = 0.65 - 0.8$ were produced but the H-mode phase, and the associated bootstrap current, could only be maintained for ~ 60 ms before the RF power tripped off. The RF power trips occurred because the plasma control system (PCS) latency was too large, so that the gap between the outer edge of the plasma and the HHFW antenna (outer gap) could not be maintained as the plasma stored energy suddenly increased at the L-mode (low-confinement) to H-mode transition (L-H transition). The resultant rapid change in outer gap after the L-H transition caused the reflected RF power to increase, resulting in the RF power being shut off. Following the shutdown of the RF power, the plasma transitioned back to the L-mode and the RF power turned on again. This “L-H-L” cycle was repeated several times during each discharge.

Since 2005, there have been improvements in the PCS, discharge conditioning, and changes in the HHFW antenna power feed design that have allowed improved RF coupling to H-mode plasmas with no NBI. This paper reports results from an experiment run in 2010 that benefited from these improvements and that demonstrated a sustained $I_p = 300$ kA, HHFW H-mode plasma that achieved a calculated $f_{NI} \sim 0.7 - 1$ with only $P_{RF} \sim 1.4$ MW, and that used CD antenna phasing.

Since 2005, the PCS latency on NSTX has been significantly reduced, and lithium conditioning has been introduced and found to increase the HHFW heating efficiency.¹⁸ Also since 2005, higher magnetic field HHFW heating experiments have been conducted at $B_T(0) = 0.55$ T, and these experiments exhibited better RF plasma coupling efficiency than experiments at $B_T(0) = 0.45$ T.¹⁹ At the higher magnetic field, the critical density for fast-wave propagation was moved further away from the front of the HHFW antenna so that RF losses to the antenna and surrounding wall structures were reduced.

The NSTX HHFW antenna is located on the outboard midplane and extends 90° toroidally. It has 12 straps connected to six decoupled 30 MHz sources that can provide up to 6 MW of RF power to the antenna. When NSTX is operated at $B_T(0) = 0.55$ T, the 30 MHz fast-waves launched by the antenna are resonant with the 7th–11th harmonics of the deuterium ion cyclotron resonance frequency. The phase shift between adjacent antenna straps can be adjusted to launch a well-defined spectrum of directed waves to generate FWCD, with launched toroidal wavenumbers, $k_\phi = \pm 13$ m⁻¹, $k_\phi = \pm 8$ m⁻¹, and $k_\phi = \pm 3$ m⁻¹, when the phase difference ($\Delta\phi$) between adjacent antenna straps is $\pm 150^\circ$, $\pm 90^\circ$, and $\pm 30^\circ$, respectively.^{18–20} Experiments reported here used $\Delta\phi = -90^\circ$ and as a result generated co- I_p FWCD, in addition to bootstrap current. In contrast, the experiments run on NSTX in 2005 used $\Delta\phi = 180^\circ$, an antenna phasing that launches a spectrum of waves with a combination of $k_\phi = \pm 14$ m⁻¹ and $k_\phi = \pm 18$ m⁻¹.

In addition to the above changes, modifications were made to the antenna between the 2005 and the 2010 HHFW

experiments reported here. The single-feed, end-grounded HHFW antenna straps originally installed on NSTX were replaced in 2009 with double-feed, center-grounded straps to reduce the RF electric fields in the vicinity of the antenna Faraday shield for a given strap current. These RF electric fields were primarily responsible for the arcs that were limiting reliable high power operation to $P_{RF} \sim 3$ MW in 2008. After the double-feed upgrade late in the 2009 NSTX run campaign, reliable operation was obtained at $P_{RF} \sim 4$ MW just after a few days of antenna conditioning.²¹ The results presented in this paper were obtained in 2010 with this new double-feed antenna configuration. Unfortunately, in 2010, the maximum arc-free P_{RF} was limited to ≤ 1.4 MW due to the accumulation of Li_2CO_3 “dust” in the antenna following multiple vents to a predominantly argon atmosphere that unintentionally included some air. The arc-free P_{RF} may also have been limited to some extent by the absence of boron conditioning at the beginning of the campaign and inter-shot glow discharge cleaning during the campaign.

Section II presents experimental and modeling results, and Sec. III discusses the implications of these results and future plans for developing $f_{NI} \geq 1$ discharges in the NSTX upgrade (NSTX-U) (Ref. 22) in 2014.

II. RESULTS

Most of the attempts to generate high f_{NI} HHFW $I_p = 300$ kA deuterium H-mode discharges in 2010 resulted in good initial RF heating and CD in the plasma core as the RF power ramped up, but core RF heating efficiency rapidly decayed soon after the L-H transition. Figure 1 summarizes the results from one of these discharges, shot 138498. The RF power was launched with a $k_\phi = -8$ m⁻¹, co- I_p CD antenna phasing, and was turned on at 0.16 s and ramped up to 1.4 MW in 100 ms, and then maintained at 1.4 MW from 0.26 s to 0.48 s (Fig. 1(b)). The outer gap was maintained at 0.08 to 0.1 m during the HHFW pulse until 0.35 s when it began oscillating between 0.05 and 0.15 m (Fig. 1(b)). If the outer gap is too large (>0.1 m), there is poor coupling to the fast wave, and if it is too small (<0.05 m), the fast wave

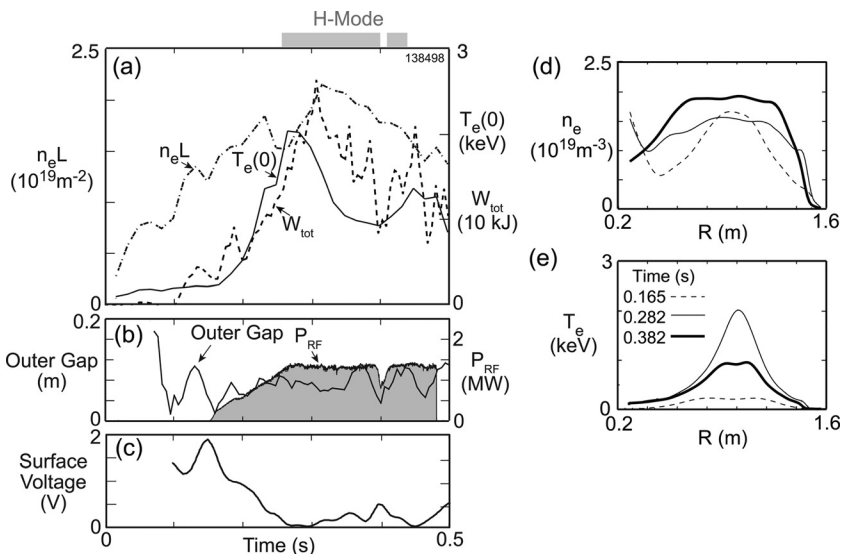


FIG. 1. Time evolution of an $I_p = 300$ kA HHFW-generated H-mode plasma (shot 138498) that did not maintain good HHFW coupling to the core during the H-mode phase. (a) Line integrated density ($n_e L$), central electron temperature ($T_e(0)$), and total plasma stored energy (W_{tot}) versus time. (b) Outer gap between the last closed flux surface and the front of the HHFW antenna on the midplane and RF power versus time. (c) The time evolution of the measured loop voltage. (d) Electron density and (e) electron temperature versus major radius at three times during shot 138498; 0.165 s (dashed line), 0.282 s (thin solid line), and 0.382 s (thick solid line).

starts propagating near the antenna so that the RF power is deposited on the antenna and surrounding vacuum vessel structures. In this case, the outer gap briefly falls below 0.05 m at 0.4 s, the reflected RF power increases, and the discharge drops out of H-mode. The loop voltage (Fig. 1(c)) initially falls to zero at the start of the flat top of the RF power but rises to 0.3–0.5 V when the outer gap fluctuates after 0.35 s. The line average density ($n_e L$) was $1.25 \times 10^{19} \text{ m}^{-2}$ at the start of HHFW heating, as measured by multi point Thomson scattering (MPTS) (Fig. 1(a), dashed line) and rises to about $2 \times 10^{19} \text{ m}^{-2}$ during the HHFW heating pulse. The central electron temperature ($T_e(0)$), measured by MPTS, (Fig. 1(a), solid line) increased from 0.2 keV at 0.16 s to 2 keV at 0.26 s as the HHFW power ramped to 1.4 MW and the plasma transitioned to H-mode. The plasma stored energy (W_{tot}) increased from 5 kJ at 0.16 s to 24 kJ at 0.3 s. After the H-mode transition, $T_e(0)$ and W_{tot} decreased to 0.9 keV and 18 kJ, respectively, at 0.38 s. Figures 1(d) and 1(e) show the evolution of the n_e profile ($n_e(R)$) and T_e profile ($T_e(R)$), respectively. At the start of HHFW heating (Fig. 1(d), 0.165 s, dashed line) $n_e(R)$ is peaked and $T_e(R)$ is flat (Fig. 1(e), 0.165 s, dashed line). At 0.282 s (thin solid line), after the H-mode transition, the $n_e(R)$ profile has flattened, the density on axis remained at $1.5 \times 10^{19} \text{ m}^{-3}$, and a relatively steep edge pedestal developed. At 0.282 s $T_e(R)$ became very peaked with a central value of 2 keV, consistent with good HHFW heating near the magnetic axis. At 0.382 s (thick solid line), $n_e(R)$ was still flat in the core with a central value of $2 \times 10^{19} \text{ m}^{-3}$, but the edge pedestal was no longer as steep and $T_e(R)$ had broadened, indicative of poor HHFW heating near the axis.

The GENRAY ray tracing code²³ and the ADJ adjoint quasi-linear Fokker-Planck code²⁴ were used to model the RF heating and CD throughout the HHFW pulse on shot 138498. Figure 2 shows results at 0.282 s, near the time of peaked $T_e(R)$ and W_{tot} . Figure 2(a) shows $T_e(r/a)$ (solid line) and $n_e(r/a)$ (dashed line) used for the modeling. 41 rays were launched at the last closed flux surface (LCFS), and these were followed until 99% of the RF power was absorbed. RF power losses in the scrape off were not included in the modeling, although these can be significant. Figure 2(b) plots the trajectory of the rays projected on the poloidal plasma cross-section. There was strong single pass RF power absorption, with the power being deposited near the midplane in the outer half of the plasma. A 3% hydrogen impurity was included, but almost all the RF power was absorbed directly by electrons through Landau damping or transit-time magnetic pumping. Figure 2(c) shows profiles of the RF power deposition (solid line) and FWCD (dashed line) versus r/a at 0.282 s for 1 MW of RF power deposition inside the LCFS. Most of the RF power is deposited inside of $r/a \sim 0.5$, but FWCD is confined to the region inside $r/a \sim 0.3$ because of the extensive region of electron trapping in NSTX. The calculated FWCD efficiency was 80 kA/MW. This corresponds to a current drive figure of merit, $\gamma_{CD} (n_e \times 10^{20} \text{ m}^{-3}) J_p (\text{A}) R_o (\text{m}) / P_{RF} (\text{W}) = 0.012 \text{ A}/(\text{Wm}^2)$. Later in time, at 0.382 s, the FWCD efficiency calculated by GENRAY-ADJ dropped to 50 kA/MW and γ_{CD} fell to $0.009 \text{ A}/(\text{Wm}^2)$, as a result of the higher n_e and lower T_e at that time. An estimate of the

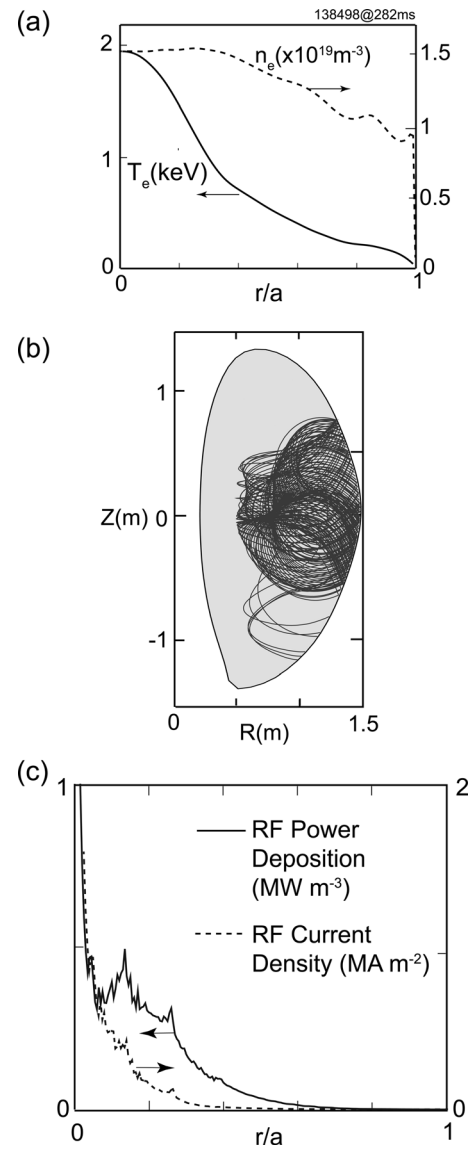


FIG. 2. (a) $n_e(r/a)$ and $T_e(r/a)$ at 0.282 s, near the time of peaked $T_e(0)$ and W_{tot} , for shot 138498. (b) GENRAY-ADJ ray trajectories plotted on a poloidal cross section for shot 138498 at 0.282 s, each ray is followed until 99% of the power is absorbed. (c) GENRAY-ADJ RF power deposition (solid line) and RF-driven current (dashed line) versus r/a at 0.282 s for shot 138498.

HHFW coupling efficiency (η_{eff}) was obtained from the time evolution of both the total plasma stored energy and the electron stored energy derived from integration of the MPTS n_e and T_e profile data using the technique described in Ref. 25. For shot 138498 $\eta_{eff} \sim 55\%$, so that at 0.282 s ~ 0.8 MW of RF power is estimated to be absorbed inside the LCFS and generates about ~ 65 kA of FWCD.

The time evolution of the RF power deposition and FWCD for shot 138498 was also modeled with a version of the TORIC full-wave code²⁶ integrated into the TRANSP transport code.²⁷ This modeling also did not include RF coupling losses outside the LCFS; namely, it assumed $\eta_{eff} = 100\%$. Figure 3 shows the time evolution of the FWCD (dashed line) and the bootstrap current (thin solid line) for shot 138498. TRANSP-TORIC predicts 100 kA of FWCD at 0.282 s, similar to the 110 kA predicted by GENRAY-ADJ, and 140 kA of bootstrap current. Assuming $\eta_{eff} \sim 55\%$, as estimated earlier, the TRANSP-TORIC

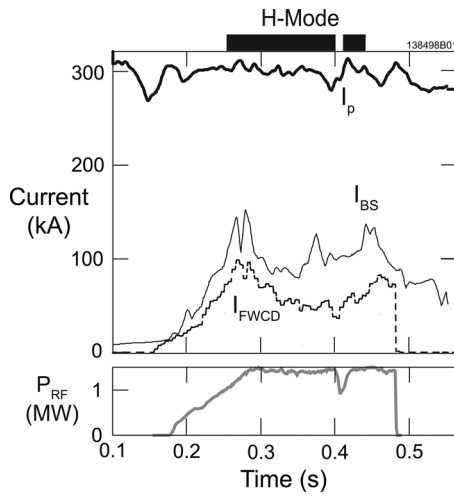


FIG. 3. I_p (thick solid black line), bootstrap current (I_{BS} , thin solid black line), and RF-driven current (I_{FWCD} , dashed line), calculated by TRANSP-TORIC, and P_{RF} (thick solid grey line) plotted as a function of time for shot 138498.

calculation implies 50 kA of FWCD, giving a total calculated non-inductive current, $I_{BS} + I_{FWCD} \sim 190$ kA, and an $f_{NI} \sim 0.65$ at 0.282 s. The time evolution of loop voltage calculated by TRANSP assuming $\eta_{eff} = 100\%$ was in close agreement with the time evolution of the measured loop voltage shown in Fig. 1(c), indicating that η_{eff} may have been somewhat higher than $\sim 55\%$ during the HHFW heating pulse, and that f_{NI} may have increased to more than ~ 0.65 at 0.282 s.

In one discharge, shot 138506, $n_e L$ before the HHFW heating pulse was reduced to $0.75 \times 10^{19} \text{ m}^{-2}$, about 40% lower than the other $I_p = 300$ kA, $B_T(0) = 0.55$ T shots run during the experiment. As a result significantly better RF core heating was obtained during the H-mode phase for a period lasting ~ 200 ms. Figure 4(a) shows the time evolution of $n_e L$, $T_e(0)$, and W_{tot} for shot 138506, and Fig. 4(b) shows the time evolution of P_{RF} and the outer gap. $n_e L$ remained lower than 138498 throughout the H-mode phase. $T_e(0)$

increased to 3 keV during the RF heating pulse, 50% higher than shot 138498, and unlike shot 138498, it kept rising until an antenna arc at 0.4 s shutdown the RF power for 20 ms. W_{tot} did not fall early in the H-mode phase, as it did during shot 138498. Notably, the outer gap stayed between 0.05 and 0.1 m throughout the RF pulse, and the discharge remained in the H-mode regime through the antenna arc at 0.4 s. The loop voltage (Fig. 4(c)) fell to close to zero between 0.3 and 0.4 s. Figure 4(d) shows four density profiles measured by MPTS during shot 138506. $n_e(R)$ remained peaked until the L-H transition at 0.21 s, at which time it developed a steep edge pedestal. At 0.29 s an internal transport barrier (ITB) formed at $r/a \sim 0.4$ and then $n_e(R)$ became hollow inside the ITB, and the loop voltage was close to zero when the ITB was present. Unfortunately, a motional Stark effect (MSE) measurement of the current density profile was not available on the day of this experiment, but it is possible that the FWCD near the core changed the local magnetic shear in the core enough to trigger the formation of the ITB. This behavior is similar to $f_{NI} \sim 1$ H-mode discharges that were generated with neutral beam injection in JT-60U when an ITB formed near a region of reversed magnetic shear.²⁸

Figure 5 shows GENRAY-ADJ results at 0.382 s, near the time of peak $T_e(0)$ and W_{tot} for shot 138506. $n_e(r/a)$ and $T_e(r/a)$ profiles used for the modeling at 0.382 s are plotted in Fig. 5(a). The 41 rays used in the calculation are plotted on the poloidal cross section in Fig. 5(b). Rays are plotted until 99% of the RF power is absorbed. As for shot 138498, there was strong single pass RF absorption of all the rays near the midplane in the outer half of the plasma, and the RF power deposition profile was peaked on axis (Fig. 5(c)). GENRAY-ADJ predicts 115 kA of co- I_p FWCD inside $r/a \sim 0.2$ for each MW of RF power deposited inside the LCFS, corresponding to $\gamma_{CD} = 0.012 \text{ A}/(\text{Wm}^2)$. η_{eff} was estimated to be $\sim 60\%$ for shot 138506, yielding ~ 90 kA of FWCD.

The time evolution of the bootstrap current and FWCD during shot 138506, calculated by TRANSP-TORIC, is plotted in

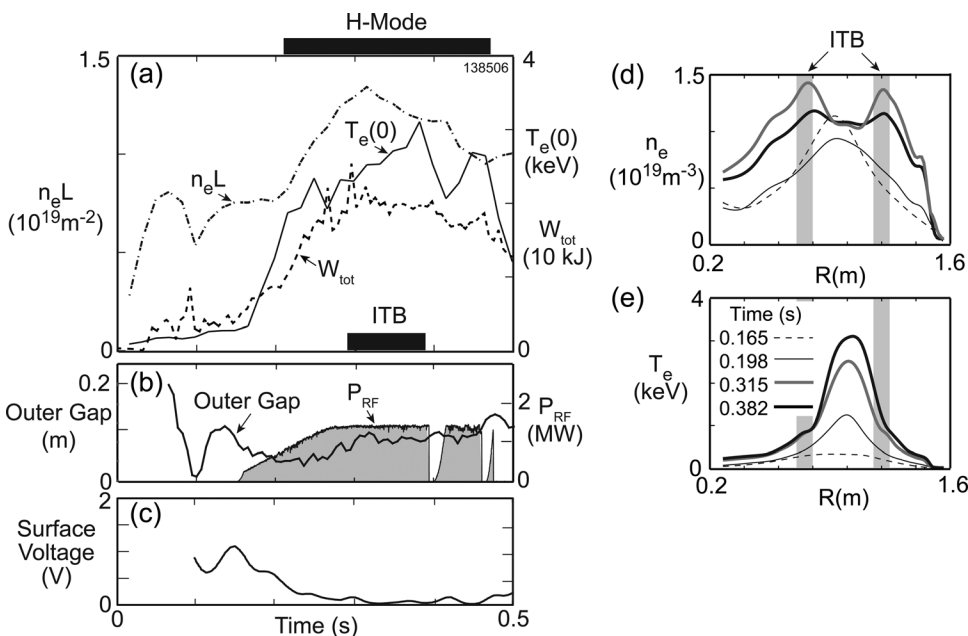


FIG. 4. Time evolution of an $I_p = 300$ kA HHFW-generated H-mode plasma (shot 138506) that maintained good HHFW coupling to the core during the H-mode phase. (a) Line integrated density ($n_e L$), central electron temperature ($T_e(0)$), and total plasma stored energy (W_{tot}) versus time. (b) Outer gap between the last closed flux surface and the front of the HHFW antenna on the midplane and RF power versus time. (c) The time evolution of the measured loop voltage. (d) Electron density and (e) electron temperature versus major radius at four times during shot 138506; 0.165 s (dashed line), 0.282 s (thin solid black line), 0.298 s (thick solid grey line), and 0.382 s (thick solid black line).

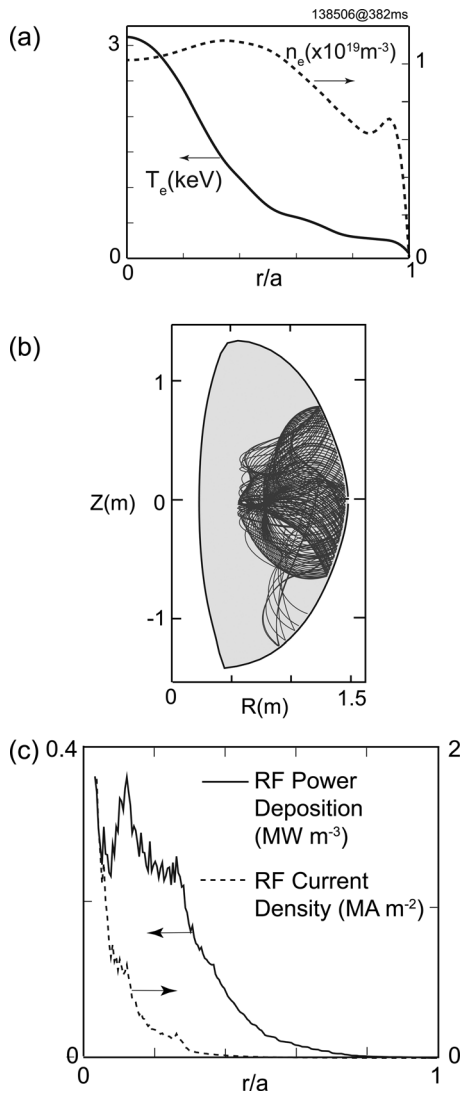


FIG. 5. (a) $n_e(r/a)$ and $T_e(r/a)$ at 0.382 s, near the time of peaked $T_e(0)$ and W_{tot} , for shot 138506. (b) GENRAY-ADJ ray trajectories plotted on a poloidal cross section for shot 138506 at 0.382 s, each ray is followed until 99% of the power is absorbed. (c) GENRAY-ADJ RF power deposition (solid line) and RF-driven current (dashed line) versus r/a at 0.382 s for shot 138506.

Fig. 6(a). Assuming $\eta_{eff} = 100\%$, 100–120 kA of FWCD is calculated to be generated during the flat top of the RF heating pulse (dashed line in Fig. 6(a)). The calculated bootstrap current oscillates between 100 and 230 kA (thin solid line in Fig. 6(a)). These large fluctuations in bootstrap current result from plasma pressure profile changes near the end of the RF power ramp-up (at 0.26 s), at the formation of the ITB (at 0.3 s) and inside the ITB (at 0.38 s) (Fig. 6(b)). Using $\eta_{eff} \sim 60\%$, $I_{FWCD} \sim 70$ kA at 0.382 s (Fig. 6(c)), slightly less than the value predicted by GENRAY-ADJ. At 0.382 s, $I_{FWCD} + I_{BS} \sim 220$ kA, yielding a calculated $f_{NI} \sim 1$. Three quarters of the non-inductive current was generated inside the ITB. As a result of the large fluctuations in bootstrap current during the H-mode phase, the calculated f_{NI} varies between 0.7 and 1. As for shot 138498, the time evolution of loop voltage calculated by TRANSP assuming $\eta_{eff} = 100\%$ was in good agreement with the time evolution of the measured loop voltage shown in Fig. 4(c).

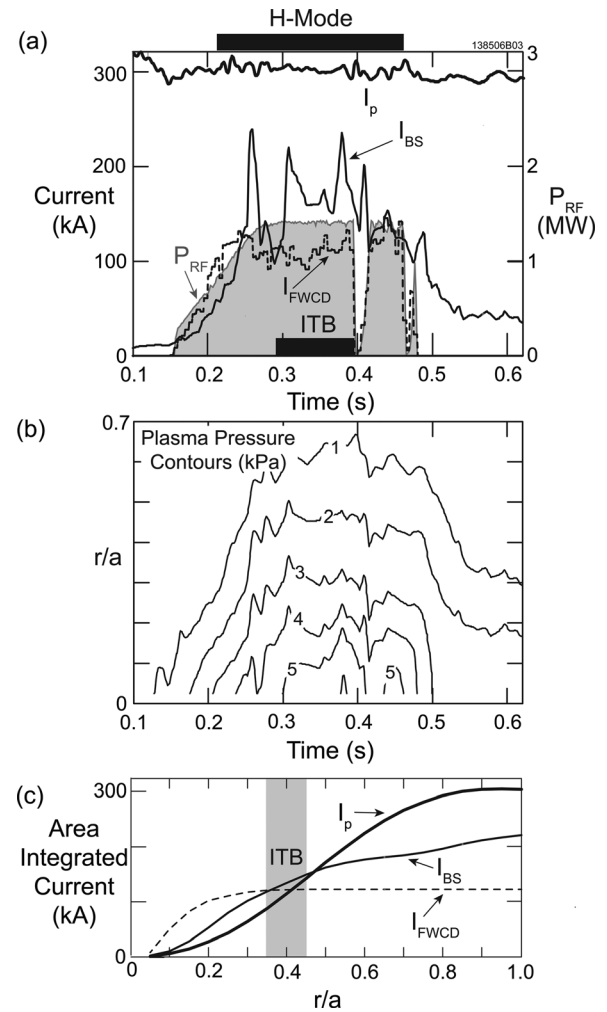


FIG. 6. (a) I_p (thick solid line), I_{BS} (thin solid line) and I_{FWCD} (dashed line) calculated by TRANSP-TORIC for shot 138506, and the RF power (Gray shading) plotted versus time. (b) Contour plot of the plasma pressure calculated by TRANSP-TORIC plotted versus r/a and time for shot 138506. Contours are plotted in kPa increments. (c) Area integrated current versus r/a calculated by TRANSP-TORIC at 0.382 s, including I_p (thick solid line), I_{BS} (thin solid line) and the I_{FWCD} (thin black line). The location of the internal transport barrier (ITB) is indicated by the shaded region near $r/a = 0.4$.

III. DISCUSSION

While the maximum arc-free HHFW P_{RF} was limited to ~ 1.4 MW in 2010 it was nevertheless possible to generate a $I_p = 300$ kA, $B_T(0) = 0.55$ T deuterium H-mode plasma with a loop voltage close to zero and a calculated $f_{NI} = 0.7 - 1$. This positive result was made possible by better outer gap control during the H-mode phase, so that the H-mode was sustained for ~ 250 ms, notably better than ~ 60 ms achieved in similar experiments in NSTX in 2005. Lower target densities, made possible in part by using lithium conditioning, operation at higher $B_T(0)$, and CD antenna phasing significantly increased the calculated f_{NI} achieved for a given P_{RF} . A calculated $f_{NI} = 0.7 - 1$ was obtained with about half the P_{RF} used in the 2005 NSTX experiments. However, there were still problems with maintaining an optimal outer gap for good HHFW coupling on many of the discharges. Even during the best discharge, shot 138506, there were large, rapid variations in bootstrap current due to changes in the core pressure profile.

Clearly, better control of the electron pressure profile is needed. In addition, MSE measurements²⁹ of the current profile are important to benchmark the TRANSP-TORIC analysis, and these were not available in 2010 on the day the experimental results reported here were acquired. Experiments originally planned for 2011 to extend the generation of HFW H-modes to higher arc-free P_{RF} in NSTX were cancelled when the NSTX experimental program was terminated due to a toroidal field coil failure. $f_{NI} \geq 1$ HFW H-mode experiments with $P_{RF} \sim 4$ MW will resume in 2014 on NSTX-U, where it will be possible to run discharges with $B_T(0)$ up to 1 T. $f_{NI} > 1$, current overdrive experiments will attempt to ramp I_p from 300 to 500 kA with HFW power alone. Also, a new MSE diagnostic that uses laser-induced fluorescence (MSE-LIF) (Ref. 30) and that uses a low-power 30 keV diagnostic neutral beam, rather than a more perturbing 90 keV high power NSTX heating beam will be available for current density profile measurements on NSTX-U.

ACKNOWLEDGMENTS

The authors wish to acknowledge the support of Dr. Masayuki Ono and Dr. Jonathan Menard, the NSTX team, and the machine and RF operations groups. This work was supported under United States Department of Energy contract numbers DE-AC02-09CH11466 and DE-AC05-00OR22725.

- ¹F. Wagner, G. Becker, K. Behringer, D. Campbell, A. Eberhagen, W. Engelhardt, G. Fussmann, O. Gehre, J. Gernhardt, G. V. Gierke, G. Haas, M. Huang, F. Karger, M. Keilhacker, O. Kluber, M. Kornherr, K. Lackner, G. Lisitano, G. G. Lister, H. M. Mayer, D. Meisel, E. R. Muller, H. Murmann, H. Niedermeyer, W. Poschenrieder, H. Rapp, H. Rohr, F. Schneider, G. Siller, E. Speth, A. Stabler, K. H. Steuer, G. Venus, O. Vollmer, and Z. Yu, *Phys. Rev. Lett.* **49**, 1408 (1982).
- ²K. Steinmetz, J.-M. Noterdaeme, F. Wagner, F. Wesner, J. Baumler, B. Becker, H. S. Bosch, M. Brambilla, F. Braun, H. Brocken, A. Eberhagen, R. Fritsch, G. Fussmann, O. Gehre, J. Gernhardt, G. v. Gierke, E. Glock, O. Gruber, G. Haas, J. Hofmann, F. Hofmeister, A. Izvozchikov, G. Janeschitz, F. Karger, M. Keilhacker, O. Kliiber, M. Kornherr, K. Lackner, G. Lisitano, E. van Mark, F. Mast, H. M. Mayer, K. McCormick, D. Meisel, V. Mertens, E. R. Muller, H. Murmann, H. Niedermeyer, W. Poschenrieder, S. Puri, H. Rapp, H. Rohr, F. Rytter, K.-H. Schmitter, F. Schneider, C. Setzensack, G. Siller, P. Smeulders, F. Soldner, E. Speth, K.-H. Steuer, O. Vollmer, H. Wedler, and D. Zasche, *Phys. Rev. Lett.* **58**, 124 (1987).
- ³N. J. Fisch and C. F. F. Karney, *Phys. Fluids* **24**, 27 (1982).
- ⁴S. C. Chiu, V. S. Chan, R. W. Harvey, and M. Porkolab, *Nucl. Fusion* **29**, 2175 (1989).
- ⁵C. C. Petty, R. I. Pinsky, M. J. Mayberry, M. Porkolab, F. W. Baity, P. T. Bonoli, S. C. Chiu, J. C. M. de Haas, R. H. Goulding, D. J. Hoffman, T. C. Luce, and R. Prater, *Phys. Rev. Lett.* **69**, 289 (1992).
- ⁶E. S. Marmor and Alcator C-Mod Group, *Fusion Sci. Technol.* **51**, 261 (2007).
- ⁷D. W. Swain and R. H. Goulding, *Fusion Eng. Des.* **82**, 603 (2007).
- ⁸E. F. Jaeger, L. A. Berry, E. F. D’Azevedo, R. F. Barrett, S. D. Ahern, D. W. Swain, D. B. Batchelor, R. W. Harvey, J. R. Myra, D. A. D’Ippolito, C. K. Phillips, E. Valeo, D. N. Smithe, P. T. Bonoli, J. C. Wright, and M. Choi, *Phys. Plasmas* **15**, 072513 (2008).
- ⁹M. Ono, M. G. Bell, R. E. Bell, T. Bigelow, M. Bitter, W. Blanchard, D. S. Darrow, E. D. Fredrickson, D. A. Gates, L. R. Grisham, J. C. Hosea, D. W. Johnson, R. Kaita, S. M. Kaye, S. Kubota, H. W. Kugel, B. P. LeBlanc, R. Maingi, R. Maqueda, E. Mazzucato, J. Menard, D. Mueller, B. A. Nelson, C. Neumeyer, F. Paoletti, S. F. Paul, Y.-K. M. Peng, S. Ramakrishnan, R. Raman, P. M. Ryan, S. A. Sabbagh, C. H. Skinner, T. Stevenson, D. Stutman, D. W. Swain, E. J. Synakowski, G. Taylor, A. Von Halle, J. Wilgen, M. Williams, J. R. Wilson, S. J. Zweben, R. Ackers, R. E. Barry, A. Bers, J. M. Bialek, P. T. Bonoli, M. D. Carter, J. Chrzanowski, W. Davis, E. J. Doyle, L. Dudek, P. C. Efthimion, R. Ellis, J. R. Ferron, M. Finkenthal, E. Fredd, T. Gibney, R. J. Goldston, R. E. Hatcher, R. J. Hawryluk, H. Hayashiya, K. W. Hill, T. R. Jarboe, S. C. Jardin, H. Ji, M. Kalish, P. LaMarche, L. L. Lao, K. C. Lee, F. M. Levinton, N. C. Luhmann, R. Majeski, J. Manickam, R. Marsala, T. K. Mau, B. McCormack, S. S. Medley, M. M. Menon, O. Mitarai, M. Nagata, N. Nishino, G. Oliaro, H. K. Park, R. Parsells, G. Pearson, T. Peebles, C. K. Phillips, R. Pinsky, G. D. Porter, A. K. Ram, J. Robinson, P. Roney, A. L. Roquemore, A. Rosenberg, M. Schaffer, S. Shiraiwa, P. Sichta, D. Stotler, B. C. Stratton, Y. Takase, W. R. Wampler, G. A. Wurden, X. Q. Xu, J. G. Yang, L. Zeng, and W. Zhu, *Nucl. Fusion* **41**, 1435 (2001).
- ¹⁰Y.-K. M. Peng and D. J. Strickler, *Nucl. Fusion* **26**, 769 (1986).
- ¹¹S. C. Jardin, N. Pomphrey, and J. DeLucia, *Comput. Phys.* **66**, 481 (1983).
- ¹²C. E. Kessel, E. J. Synakowski, M. E. Bell, D. A. Gates, R. W. Harvey, S. M. Kaye, T. K. Mau, J. Menard, C. K. Phillips, G. Taylor, R. Wilson, and the NSTX Research Team, *Nucl. Fusion* **45**, 814 (2005).
- ¹³P. M. Ryan, A. L. Rosenberg, D. W. Swain, J. R. Wilson, D. B. Batchelor, M. G. Bell, R. E. Bell, S. Bernabei, J. M. Bitter, P. T. Bonoli, M. Brambilla, A. Cardinali, M. D. Carter, D. Darrow, E. Frederickson, D. Gates, J. C. Hosea, E. F. Jaeger, S. M. Kaye, B. P. LeBlanc, R. Maingi, T. K. Mau, S. S. Medley, J. E. Menard, D. Mueller, M. Ono, F. Paoletti, Y.-K. M. Peng, C. K. Phillips, R. I. Pinsky, D. A. Rasmussen, S. A. Sabbagh, E. J. Synakowski, J. B. Wilgen, and NSTX Team, in *Proceedings of the 19th IAEA Fusion Energy Conference, Lyon, 2002*, edited by M. Spak, IAEA, Vienna, 2003, Paper No. EX/P2-13.
- ¹⁴R. Raman, D. Mueller, T. R. Jarboe, B. A. Nelson, M. G. Bell, M. Ono, T. Bigelow, R. Kaita, B. LeBlanc, K. C. Lee, R. Maqueda, J. Menard, S. Paul, and L. Roquemore, *Nucl. Fusion* **47**, 792 (2007).
- ¹⁵W. Choe, J. Kim, and M. Ono, *Nucl. Fusion* **45**, 1463 (2005).
- ¹⁶D. J. Battaglia, M. W. Bongard, R. J. Fonck, A. J. Redd, and A. C. Sontag, *J. Fusion Energy* **28**, 140 (2009).
- ¹⁷C. E. Kessel, R. E. Bell, M. G. Bell, D. A. Gates, S. M. Kaye, B. P. LeBlanc, J. E. Menard, C. K. Phillips, E. J. Synakowski, G. Taylor, R. Wilson, and NSTX Research Team, *Phys. Plasmas* **13**, 056108 (2006).
- ¹⁸G. Taylor, R. E. Bell, J. C. Hosea, B. P. LeBlanc, C. K. Phillips, M. Podesta, E. J. Valeo, J. R. Wilson, J.-W. Ahn, G. Chen, D. L. Green, E. F. Jaeger, R. Maingi, P. M. Ryan, J. B. Wilgen, W. W. Heidbrink, D. Liu, P. T. Bonoli, T. Brecht, M. Choi, and R. W. Harvey, *Phys. Plasmas* **17**, 056114 (2010).
- ¹⁹J. C. Hosea, R. E. Bell, B. P. LeBlanc, C. K. Phillips, G. Taylor, E. Valeo, J. R. Wilson, E. F. Jaeger, P. M. Ryan, J. Wilgen, H. Yuh, F. Levinton, S. Sabbagh, K. Tritz, J. Parker, P. T. Bonoli, R. Harvey, and NSTX Team, *Phys. Plasmas* **15**, 056104 (2008).
- ²⁰C. K. Phillips, R. E. Bell, L. A. Berry, P. T. Bonoli, R. W. Harvey, J. C. Hosea, E. F. Jaeger, B. P. LeBlanc, P. M. Ryan, G. Taylor, E. J. Valeo, J. B. Wilgen, J. R. Wilson, J. C. Wright, H. Yuh, and the NSTX Team, *Nucl. Fusion* **49**, 075015 (2009).
- ²¹P. M. Ryan, R. Ellis, J. C. Hosea, C. C. Kung, B. P. LeBlanc, R. I. Pinsky, G. Taylor, J. R. Wilson, and the NSTX Team, *AIP Conf. Proc.* **1406**, 101 (2011).
- ²²J. E. Menard, J. Canik, B. Covele, S. Kaye, C. Kessel, M. Kotschenreuther, S. Mahajan, R. Maingi, C. Neumeyer, M. Ono, R. Raman, S. Sabbagh, V. Soukhanovskii, and P. Valanju, in *Proceedings of the 37th European Physical Society Conference on Plasma Physics* (Dublin, Ireland, 2010), paper P2.106.
- ²³A. P. Smirnov and R. W. Harvey, *Bull. Am. Phys. Soc.* **40**, 1837 (1995).
- ²⁴A. P. Smirnov, R. W. Harvey, and R. Prater, in *Proceedings of the 15th Workshop on ECE and ECRH* (World Scientific, 2009), pp. 301–306.
- ²⁵J. C. Hosea, S. Bernabei, T. Biewer, B. LeBlanc, C. K. Phillips, J. R. Wilson, D. Stutman, P. Ryan, and D. W. Swain, *AIP Conf. Proc.* **787**, 82 (2005).
- ²⁶M. Brambilla, *Plasma Phys. Control. Fusion* **44**, 2423 (2002).
- ²⁷R. J. Hawryluk, in “Physics of plasmas close to thermonuclear conditions,” in *Proceedings of the International School of Plasma Physics* (Pergamon, Varenna, Italy, 1981) Vol. **1**, p. 19.
- ²⁸T. Fujita, S. Ide, Y. Kamada, T. Suzuki, T. Oikawa, S. Takeji, Y. Sakamoto, Y. Koide, A. Isayama, T. Hatae, H. Kubo, S. Higashijima, O. Naito, H. Shirai, and T. Fukuda, *Phys. Rev. Lett.* **87**, 085001 (2001).
- ²⁹F. M. Levinton, R. J. Fonck, G. M. Gammel, R. Kaita, H. W. Kugel, E. T. Powell, and D. W. Roberts, *Phys. Rev. Lett.* **63**, 2060 (1989).
- ³⁰E. L. Foley and F. M. Levinton, *Rev. Sci. Instrum.* **77**, 10F311 (2006).